RSC Sustainability

ROYAL SOCIETY OF CHEMISTRY

PAPER

View Article Online
View Journal | View Issue

Cite this: *RSC Sustainability*, 2023, **1**, 1861

A techno-economic approach to guide the selection of flow recyclable ionic liquids for nanoparticle synthesis†

Lanja R. Karadaghi, [a] Bin Pan, [b] Frederick G. Baddour, *[c] Noah Malmstadt *[abde] and Richard L. Brutchey *[a]

Received 8th June 2023
Accepted 10th September 2023

DOI: 10.1039/d3su00182b

rsc.li/rscsus

Ionic liquids (ILs) are an important class of solvents that can be sustainable alternatives to conventional volatile organic solvents owing to their non-flammability, negligible vapor pressures, and high thermal and chemical stabilities. While several advantages to employing ILs as reaction solvents in colloidal inorganic nanoparticle syntheses have been demonstrated, their significantly higher purchase costs compared to traditional organic solvents creates a large barrier in utilizing them at scale. However, a unique characteristic of ILs is their potential to be recycled and reused in subsequent nanoparticle reactions, which may offer a potential cost offset by reducing the amount of solvent needed over the lifetime of a process. Herein, we report an experimentally guided, early-stage techno-economic analysis of a model platinum nanoparticle synthesis using a matrix of six different ILs as the reaction solvent. A continuous flow membrane separation system was used for the purification of the ILs using acidified water, allowing both water-immiscible and water-miscible ILs to be recycled. Unsurprisingly, each of these ILs have different bulk prices, however, this synthesis-driven economic analysis revealed the impact of the synthetic consequences of varying the IL solvent system, such as different nanoparticle yields and variable solvent recoveries based on their water miscibility.

Sustainability spotlight

Ionic liquids (ILs) are sustainable solvent alternatives to conventional volatile organic solvents because they are non-flammable and have negligible vapor pressures. ILs can also be recycled and reused, thereby decreasing solvent impact and waste. This has caused them to be explored as solvents for the more sustainable synthesis of colloidal nanoparticles. Unfortunately, their high purchase cost compared to volatile organic solvents hinders widescale use. We report an experimentally guided, early-stage techno-economic analysis to discover how various factors affect the overall synthesis cost to best guide the choice of IL solvent. This analysis provides the context in which ILs can be economically adapted at scale to realize their sustainability advantages. This works aligns with the UN SDG:9, SDG:12, and SDG:13.

Introduction

Room-temperature ionic liquids (ILs) possess many unique properties that enable their use as sustainable solvent replacements for traditional volatile organic compound (VOC) solvents.[1] In direct contrast to VOCs, ILs have negligible vapor pressures (*ca.* 10^{-10} Pa at 25 °C) and are non-flammable, mitigating their emissions into the atmosphere and making them safer to handle.[2] ILs also possess high thermal and chemical stabilities, and have the potential to be recovered, recycled, and reused.[3,4] The variety of anion and cation combinations that are possible in ILs allow them to be tailored to diverse functional properties, including solubility, density, hydrophobicity, and viscosity, making them excellent task-specific solvents.[1,3,5]

The unique properties of ILs have resulted in their use as sustainable solvent alternatives for the fabrication of colloidal inorganic nanoparticles. Colloidal nanoparticles have large surface-area-to-volume ratios, unique optoelectronic properties, and large biological uptake, among other properties, enabling their use in a wide range of applications including catalysis and biomedicine.[6] Specifically, the colloidal synthesis of nanoparticles enables control over particle size, size dispersity, and

[a]*Department of Chemistry, University of Southern California, Los Angeles, California 90089, USA. E-mail: brutchey@usc.edu*

[b]*Mork Family Department of Chemical Engineering and Materials Science, University of Southern California, Los Angeles, California 90089, USA. E-mail: malmstad@usc.edu*

[c]*Catalytic Carbon Transformation and Scale-Up Center, National Renewable Energy Laboratory, Golden, Colorado 80401, USA. E-mail: frederick.baddour@nrel.gov*

[d]*Department of Biomedical Engineering, University of Southern California, Los Angeles, California 90089, USA*

[e]*USC Norris Comprehensive Cancer Center, University of Southern California, 1441 Eastlake Ave, Los Angeles, California 90033, USA*

† Electronic supplementary information (ESI) available. See DOI: https://doi.org/10.1039/d3su00182b

morphology, resulting in well-defined particles that can be tuned for the aforementioned applications.[7] When ILs are employed in colloidal nanoparticle syntheses, their low interfacial tension facilitates rapid nucleation rates, resulting in small, well-defined particles.[8] Additionally, their high dielectric constant and ionic charge can stabilize the nanoparticle surfaces through electrostatic effects, preventing agglomeration and Ostwald ripening, while also supporting high colloid concentrations.[8–12]

Despite these benefits, the largest barrier to the wide-spread implementation of ILs as reaction solvents is in their high cost compared to traditional VOC solvents, often exceeding $800/kg.[13] These significantly higher costs make the use of IL solvents economically impracticable despite their sustainability advantages over VOC solvents. This can be mitigated by the unique liquid–liquid phase separation behavior of ILs, which in some cases may allow for their extractive purification, separation, and recycling.[14] Although attempts to recycle traditional long-chain aliphatic solvents used in nanoparticle syntheses have been demonstrated,[15] it has been reported that some of these solvents (*e.g.*, 1-octadecene) go through structural degradation upon use and recycling.[16,17]

While there have been several demonstrations of successful IL recycling through multiple nanoparticle synthesis reactions,[18–23] it was not until recently that a techno-economic analysis was performed that evaluated the effects of recycling on the cost of Pt nanoparticle manufacturing using 1-butyl-3-methylimidizolium bis(trifluoromethylsulfonyl)imide (BMIM-NTf_2).[17] The study established that recycling BMIM-NTf_2 through a by-hand, batch washing and recycling process makes it cost competitive with a conventional organic solvent used in nanoparticle synthesis. While this set the precedent for recycling ILs to lower overall process cost, it is unclear how universal this result was, as various ILs will have different bulk costs, will result in different nanoparticle yields, and will have varying abilities to be purified, separated, and recycled. Because of these confounding variables, evaluating the total process economics for a specific reaction with IL solvent recovery is non-trivial.

Herein, we performed a combined experimental–economic approach utilizing a model colloidal Pt nanoparticle synthesis with a matrix of six IL solvents, where the ILs are purified, separated, and recovered using an automatic, continuous flow process. Micro- and millifluidic continuous flow processes offer various mixing-enhanced configurations for aqueous IL extraction *via* mass transfer (*e.g.*, zigzag channels[24,25] and staggered herringbone ridges[26–28]). The extraction process is serially coupled with membrane-based IL-water separation, which harnesses the differential wettability of polymeric membranes to process various liquid–liquid mixtures.[29,30] This comprehensive experimentally driven cost analysis gives vital information about how various factors affect the overall synthesis cost to best guide the choice of task-specific IL. The cost influence of synthetic outcomes that arise when varying the IL solvent (*e.g.*, isolated Pt nanoparticle yield, solvent cost, and solvent recyclability based on water miscibility) is evaluated and unlocks the identification of a process-cost assessment, which is imperative for adapting this sustainable class of solvent alternatives at scale.

Results and discussion

Pt nanoparticle synthesis

The colloidal Pt nanoparticle synthesis, modified from previously reported methods,[17,23] is based on the polyol reduction of K_2PtCl_4 with ethylene glycol in an IL solvent with a supporting polyvinylpyrrolidone (PVP) surfactant. Briefly, a solution of K_2PtCl_4 dissolved in ethylene glycol was quickly injected into a hot solution of PVP dissolved in IL at 150 °C. The resulting single-phase solution was allowed to react for 30 min before being removed from the heat source and thermally quenched in an ice bath. The reaction conditions were not specifically optimized for any of the ILs but rather held constant so a direct comparison could be made between the different IL solvents. The following IL solvents resulted in phase-pure Pt nanoparticles: 1-butyl-3-methylimidizolium bis(trifluoromethylsulfonyl) imide (BMIM-NTf_2), 1-butyl-3-methylimidizolium trifluoromethanesulfonate (BMIM-OTf), 1-butyl-1-methylpyrrolidinium bis(trifluoromethylsulfonyl)imide (BMPYRR-NTf_2), 1-butyl-1-methylpyrrolidinium trifluoromethanesulfonate (BMPYRR-OTf), 1-butyl-2-methylpyridinium bis(trifluoromethylsulfonyl)imide (BMPY-NTf_2), and 1-butyl-2-methylpyridinium trifluoromethanesulfonate (BMPY-OTf). Ten other IL solvents (listed in Table S1, ESI†) were evaluated for this reaction but did not yield isolable, phase pure Pt nanoparticles. These ILs consisted of various other combinations of phosphonium, imidazolium, pyrrolidinium, and pyridinium cations with decanoate, dicyanamide, bis(trifluoromethanesulfonate)imide, hexafluorophosphate, tetrafluoroborate, bromide, and phosphinate anions.

The separation of the Pt nanoparticles from the IL solvent is dependent on the room temperature miscibility of the IL with the ethylene glycol reducing agent. For this matrix of six ILs, the room temperature miscibility is governed by the anion, regardless of the cation. The three ILs with the NTf_2^- anion are immiscible with ethylene glycol, while the three ILs with the OTf^- anion are miscible with ethylene glycol. Differences in IL miscibility with polar solvents (*e.g.*, ethylene glycol and water) are predominantly influenced by the anion of a given IL.[31] It was recently demonstrated that the size of the IL anion plays a role in miscibility. For example, water interactions are stronger with smaller ions (OTf^-) compared to larger ions (NTf_2^-).[32] For the Pt nanoparticle syntheses in BMIM-NTf_2, BMPYRR-NTf_2, and BMPY-NTf_2 solvents, the IL phase cleanly separates from the ethylene glycol layer that contains the dispersion of Pt nanoparticles. For Pt nanoparticle syntheses in BMIM-OTf, BMPYRR-OTf, and BMPY-OTf solvents, there is no phase separation between the IL and ethylene glycol, requiring the Pt nanoparticles be isolated from these ILs through precipitation with an antisolvent (*i.e.*, acetone). The nanoparticles were then separated from the solvent mixture by centrifugation followed by recovery of the ILs by removing the VOCs *in vacuo*. In all cases, the Pt nanoparticles were worked up identically after appropriate separation from the ILs.

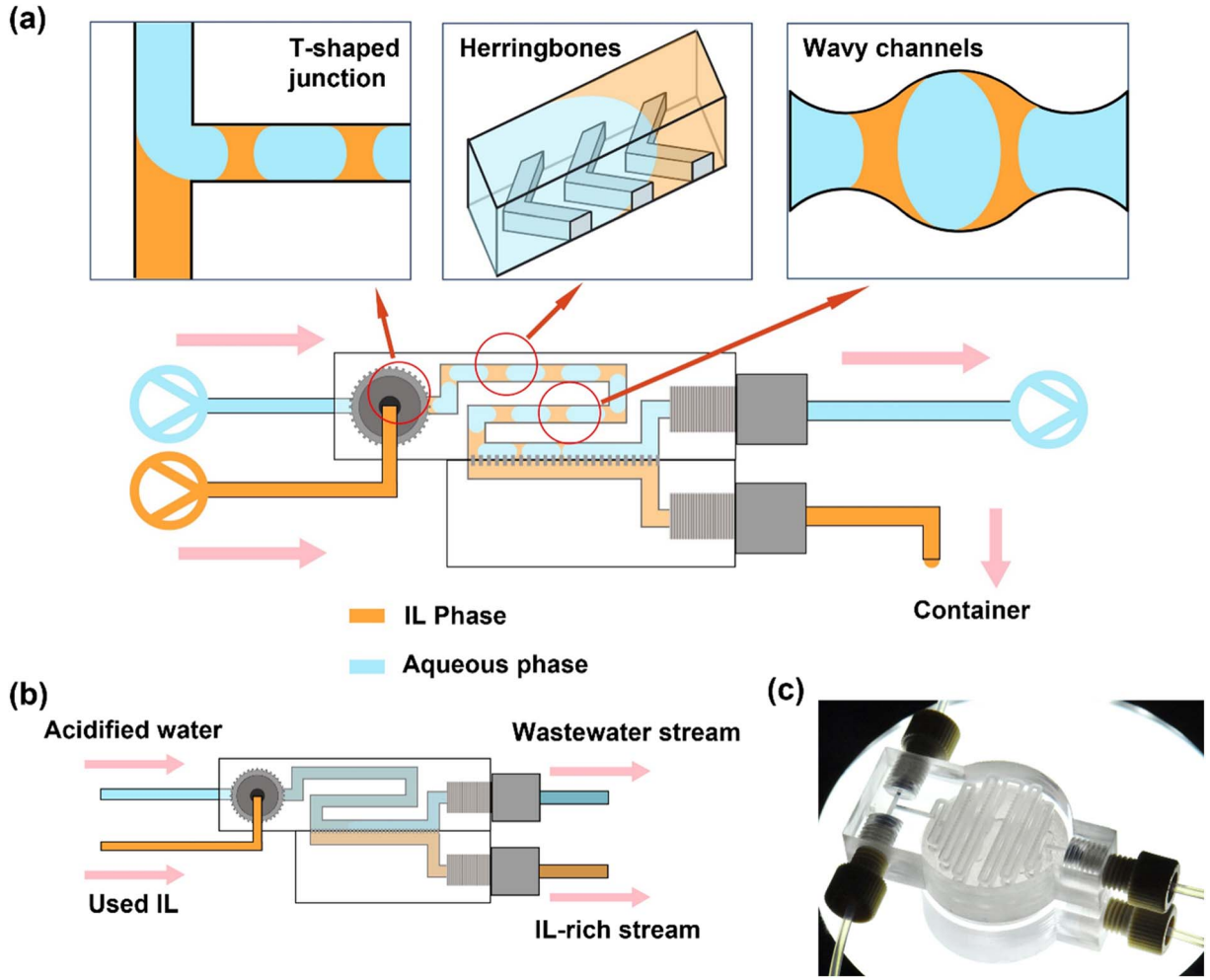

Fig. 1 Continuous flow process for used IL solvent extraction and separation. (a) Schematic drawing for recycling of the water-immiscible IL solvents with NTf_2^- anions. The used IL and acidified water streams are infused to the recycler by two syringe pumps and form slug flows in a T-shaped junction. Extraction occurs by mass transfer in herringbone-patterned channels and wavy channels downstream. The liquid–liquid biphasic flow is next separated by a membrane separator. The wastewater stream is collected by a syringe pump in withdrawal mode, while the purified IL stream is collected for reuse. (b) Partial schematic for washing the water-miscible IL solvents with OTf^- anions. A single-phase flow is formed in the T-junction. After co-flow, the IL-rich product stream is separated downstream by transport across an IL-impregnated membrane. (c) Photograph of the 3D-printed recycler.

Ionic liquid purification and recovery

Once isolated, the IL solvents may contain reaction byproducts, such as unreacted Pt salts and ethylene glycol, excess PVP, and/or oxidation products of ethylene glycol. To purify the recovered IL solvents, they were passed through an automated continuous flow recycler that first contacts the IL with an acidified aqueous phase for extraction, followed by separation of the IL phase from the aqueous phase using a membrane separator (Fig. 1). It has been demonstrated that Pt^{2+} can be stripped from ILs under acidic conditions.[33–35] For this reason, we used 0.1 M HNO_3 to wash the used ILs in the continuous flow recycler, integrating extraction (*via* mixing) and separation, adapted from a previous study.[36] All six ILs were serially washed 3× in flow with identical flow rates to complete a purification cycle, corresponding to a typical 3× wash in a by-hand batch workup.

To recycle the three water-immiscible IL solvents with NTf_2^- anions, a two-phase slug flow configuration was formed from the used IL and acidified water in a T-shaped junction (Fig. 1a). The liquid–liquid slug flow passed through a length of herringbone-patterned channel to promote mass transport and a length of wavy channel where extraction of multiple reaction byproducts occurs. In microchannels, passive interfacial diffusion of the extractants at low Reynolds numbers (*i.e.*, laminar flows) is slow. The staggered herringbone pattern on the channel introduces chaotic mixing with the existence of different boundary conditions between the ridges (non-slip) and the grooves (some-slip).[26] Channels with wavy walls introduce a velocity profile in the *y*-direction (perpendicular to the flow direction), which is absent from the flow in straight channels where only the velocity in the *x*-direction (the flow direction) exists. The convective mixing can also be enhanced by the "widening" and "narrowing" effects of the wavy pattern on the liquid–liquid biphasic flow.[37] After extraction, the slug flow entered the separation section where a hydrophobic PTFE

membrane selectively allowed the IL phase to permeate and be collected. The acidified aqueous stream carrying the impurities was retained in the upper channel. Offline, batch vacuum drying was used to remove residual water in the recovered IL recycled, since even upon perfect separation and low miscibility, trace amounts of water can still be dissolved in the IL.[38,39] Using this continuous flow purification technique, up to 94 vol% of the starting IL solvent used in the prior Pt

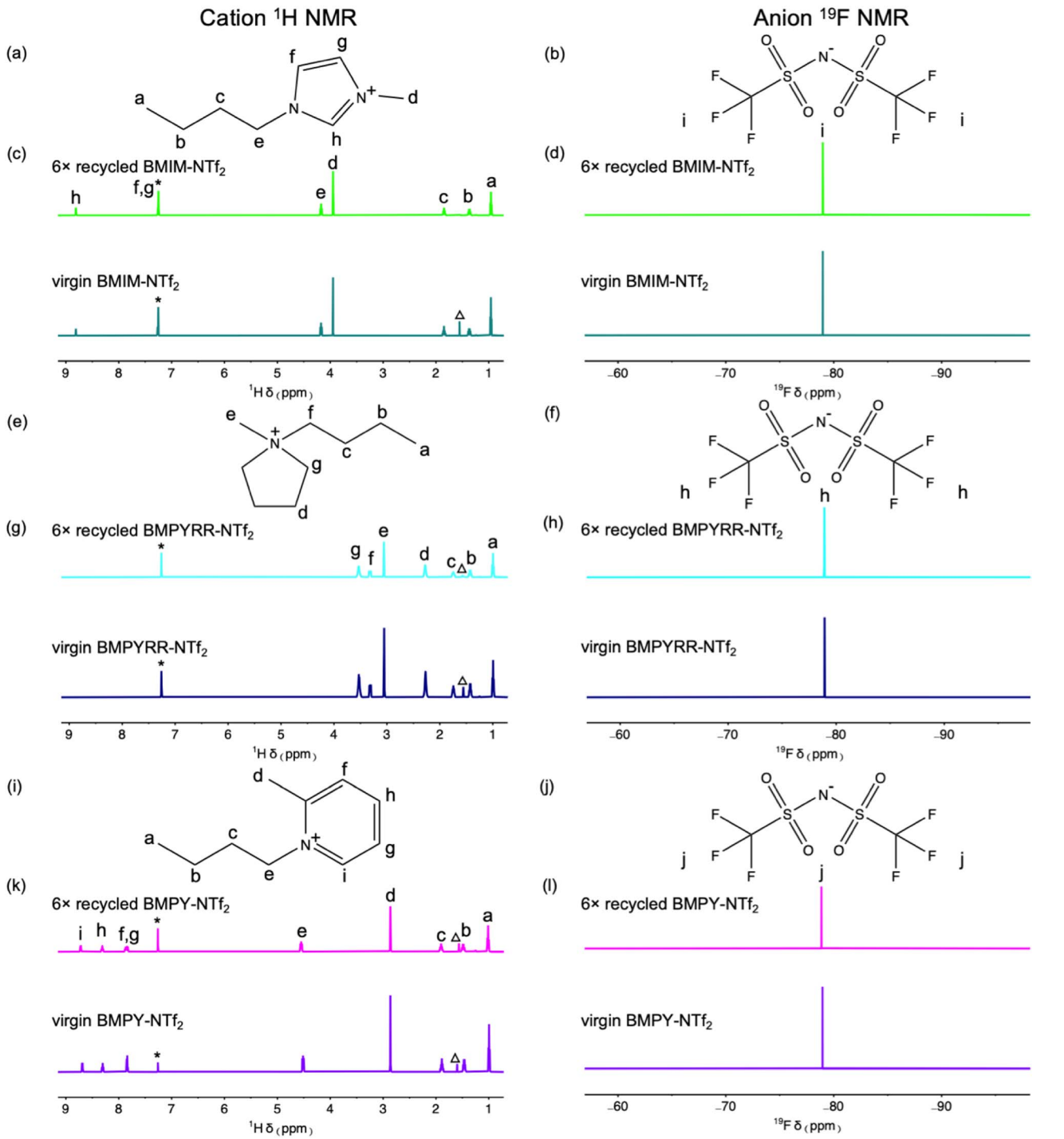

Fig. 2 Structures of the (a) $BMIM^+$ cation and the (b) NTf_2^- anion with labeled (c) solution ^{1}H NMR and (d) ^{19}F NMR spectra of virgin and 6× recycled BMIM-NTf_2. Structures of the (e) $BMPYRR^+$ cation and the (f) NTf_2^- anion with labeled (g) solution ^{1}H NMR and (h) ^{19}F NMR spectra of virgin and 6× recycled BMPYRR-NTf_2. Structures of (i) $BMPY^+$ cation and the (j) NTf_2^- anion with labeled (k) solution ^{1}H NMR and (l) ^{19}F NMR spectra of virgin and 6× recycled BMPY-NTf_2. The open triangle (△) denotes water at 1.56 ppm, as these spectra were taken before the vacuum drying step. The water content in all cases is no more than that in the as-received virgin ILs (before drying). Asterisks (*) represent the residual nondeuterated solvent peak of chloroform.

Table 1 Summary of the isolated yield, average nanoparticle size,[a] and dispersity of the Pt nanoparticles synthesized in IL solvents with NTf_2^- anions

Ionic liquid	Isolated yield (%)	Size (nm)	σ/d (%)
Virgin BMIM-NTf_2	36	3.3	18
1× recycled BMIM-NTf_2	44	3.4	14
5× recycled BMIM-NTf_2	38	3.9	16
Virgin BMPYRR-NTf_2	98	3.9	13
1× recycled BMPYRR-NTf_2	96	4.0	14
5× recycled BMPYRR-NTf_2	98	3.7	13
Virgin BMPY-NTf_2	24	1.9	15
1× recycled BMPY-NTf_2	30	2.2	16
5× recycled BMPY-NTf_2	31	2.3	18

[a] Average size was determined by measuring nanoparticle diameters from TEM images using ImageJ, a pixel-counting software ($N = 300$).

nanoparticle reaction is recovered. The dissolved water content prior to vacuum drying is <2 wt% through each recycle, as determined thermogravimetrically before and after drying.

Using this approach, we recycled and reused the same BMIM-NTf_2, BMPYRR-NTf_2, and BMPY-NTf_2 solvents for up to six Pt nanoparticle syntheses. The solution ^1H and ^{19}F NMR spectra comparing the unused, virgin ILs to the 6× recycled ILs (recovered from the last Pt nanoparticle reaction using 5× recycled IL) demonstrate that no chemical changes or degradation arise from continuous recycling and subsequent reuse of the ILs as reaction solvents (Fig. 2). The resonances spanning from δ 0.95–8.81 ppm for the $BMIM^+$ cation, δ 0.99–3.53 ppm for the $BMPYRR^+$ cation, and δ 1.01–8.69 ppm for the $BMPY^+$ cation do not change upon recycling the IL six consecutive times. The presence of a single resonance in the ^{19}F NMR spectra confirms the NTf_2^- and OTf^- anions also remain unchanged throughout the recycling process. Additionally, there are no reaction byproduct impurities observed by NMR spectroscopy after

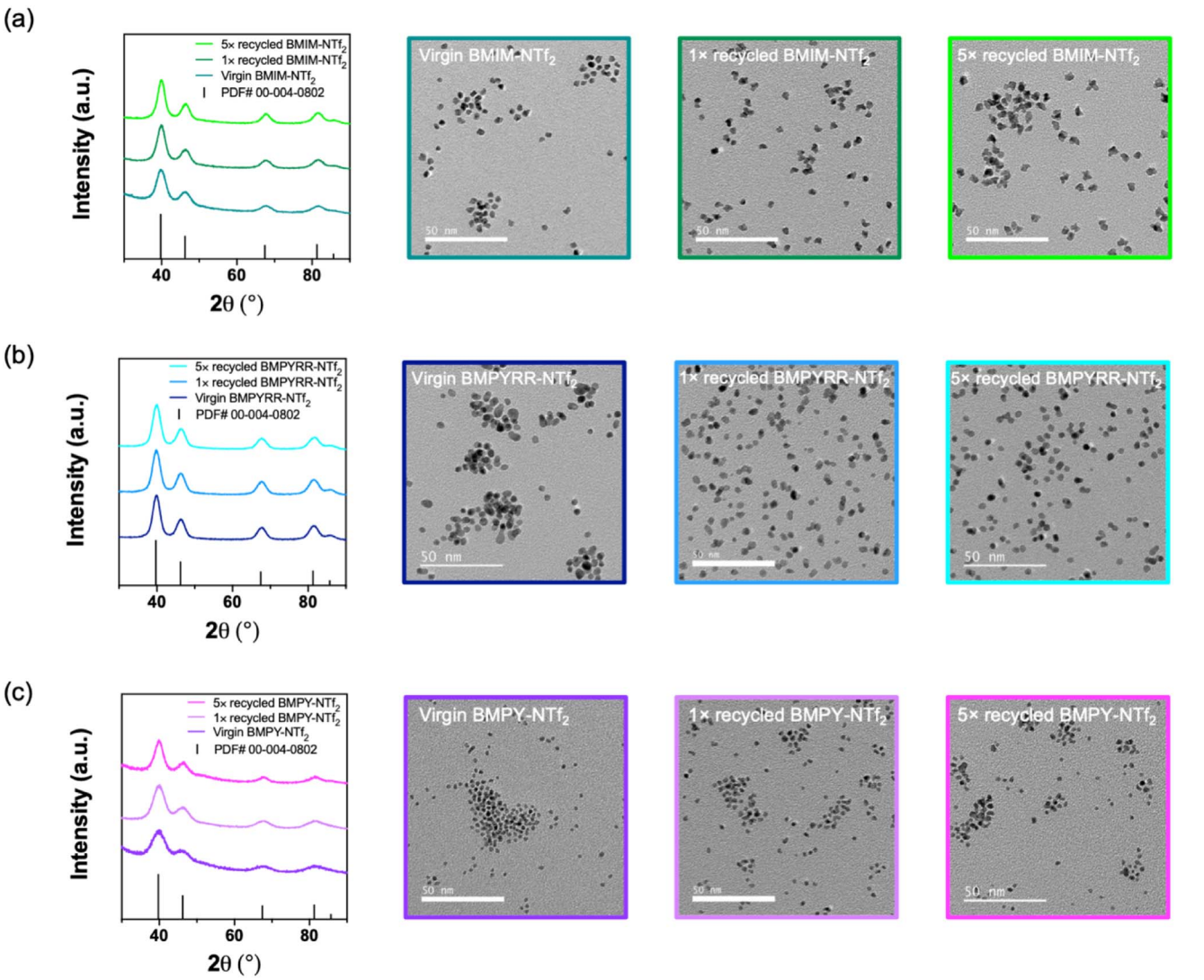

Fig. 3 Powder XRD patterns and TEM images of Pt nanoparticles synthesizing in virgin, 1× and 5× recycled (a) BMIM-NTf_2, (b) BMPYRR-NTf_2, and (c) BMPY-NTf_2.

purification and recovery. Table 1 summarizes the isolated yields of Pt nanoparticles, average nanoparticle sizes, and standard deviation about the mean diameter for the Pt nanoparticles synthesized in BMIM-NTf_2, BMPYRR-NTf_2, and BMPY-NTf_2 solvents.

A total of six Pt nanoparticle syntheses were performed with each IL, one with the virgin IL and then five subsequent reactions with recycled IL. Using the recycled IL solvents with NTf_2^- anions does not affect the Pt nanoparticle crystallinity, size, or quality, as demonstrated by the powder X-ray diffraction (XRD) patterns and the transmission electron microscopy (TEM) images (Fig. 3). The XRD patterns and TEM images for the Pt nanoparticles synthesized in virgin, 1× recycled, and 5× recycled BMIM-NTf_2, BMPYRR-NTf_2, and BMPY-NTf_2 are given in Fig. 3a–c, respectively. The XRD patterns confirm the synthesis of phase pure, face-centered cubic Pt nanoparticles throughout all experiments with recycled ILs. The average calculated lattice parameter of each product is $a = 3.89$ Å, which is in agreement with bulk Pt metal (PDF #00-004-0802). Scherrer analysis indicates a grain size of 3.8–4.1 nm for Pt nanoparticles synthesized in virgin, 1× recycled, and 5× recycled BMIM-NTf_2, 4.0–4.5 nm for Pt nanoparticles synthesized in virgin, 1× recycled, and 5× recycled BMPYRR-NTf_2, and 1.8–2.1 nm for Pt nanoparticles synthesized in virgin, 1× recycled, and 5× recycled BMPY-NTf_2. The average sizes and size dispersities are reported in Table 1, which were determined by analyzing TEM images using at least 300 nanoparticles. The TEM images of Pt nanoparticles synthesized in each virgin, 1× recycled, and 5× recycled IL show no significant size or morphology changes, as the average sizes for all the nanoparticle ensembles are well within a standard deviation of each other for each respective IL. Moreover, the sizes calculated by TEM analysis are in agreement with the grain sizes calculated by Scherrer analysis, suggesting single crystalline nanoparticles. The main difference between these three IL solvents is the isolated Pt nanoparticle yield. BMIM-NTf_2 results in an isolated Pt nanoparticle yield of 36%, BMPYRR-NTf_2 results in an isolated yield of 98%, and BMPY-NTf_2 results in an isolated yield of 24%. The isolated yield remains consistent after using 1× and 5× recycled ILs with the NTf_2^- anion, as reported in Table 1. This consistency can be attributed to the successful purification of these ILs in the continuous flow membrane separator, with no obvious carryover of Pt-containing species (*vide infra*). The successful purification of the IL solvents with the NTf_2^- anion in the continuous flow membrane separator is a direct result of their immiscibility with water.

In contrast, the IL solvents with OTf^- anions are miscible with water, making it impossible to accomplish the purification and recovery of these ILs using the legacy by-hand batch methods that rely on phase separation.[17] Distillation is a well-established approach to separate miscible liquid–liquid mixtures *via* different boiling points; however, it is not applicable to this process because unwanted, non-volatile byproducts will all remain in the IL phase. One feasible pathway to separate the miscible liquid–liquid mixture is the use of IL membrane separators.[40–42] In an IL membrane separator, a polymeric membrane is pre-wetted by a hydrophobic IL that preferably allows organic molecules to enter, while water and water-soluble impurities are partially excluded from permeation.

We employed the same extraction and separation configuration used to recycle the three IL solvents with NTf_2^- anions for recycling the water-miscible IL solvents with OTf^- anions, with the addition of a pre-treatment step to wet the membrane in the continuous flow recycler with a hydrophobic NTf_2^- IL. In each case, the IL with NTf_2^- anions used to pre-wet the membrane had the same cation as the IL with OTf^- anions to be purified to minimize any effects of mixed cations on the subsequent Pt nanoparticle syntheses. The IL infusion flow rate was kept the same as that in the NTf_2^- IL cases, while the acidified water infusion flow rate was reduced here for the OTf^- IL cases, for the purpose of alleviating the workload of downstream separation and maximizing the IL recovery rates. In the flow process, while no slug flow with two distinct phases was formed after the T-junction, the two as-described mixing configurations still served to provide thorough mixing of the water and IL (Fig. 1b). The resulting single-phase mixture was then separated by the IL-pre-wetted membrane. This resulted in an anion impurity that was difficult to separate. Consequently, the fraction of the NTf_2^- IL that was carried over to the recovered OTf^- IL resulted in the presence of two resonances in the solution ^{19}F NMR spectra of the ILs after purification and separation (Fig. S1, ESI†). Through integration of the two peaks in ^{19}F NMR,[43,44] the resulting IL contains *ca.* 2% of the NTf_2^- anion. Separation of the IL solvents with OTf^- anions and water was less efficient in this case, with subsequent vacuum drying being required to remove *ca.* 30 wt% water that remained with the permeate stream (*cf.* <2 wt% for the IL solvents with NTf_2^- anions). Using this IL-membrane purification technique, up to 70 vol% of the starting IL solvent used in the prior Pt nanoparticle reaction is recovered.

The difficulty in separating the IL solvents with the OTf^- anions from water also resulted in poorer purification of these ILs after each recovery and recycle. Fig. S1 in the ESI† shows the solution ^1H and ^{19}F NMR spectra comparing the unused virgin ILs to the 1× and 6× recycled ILs. These spectra demonstrate that the ILs remain chemically stable throughout the continuous recycling and subsequent reuse, as all the resonances corresponding to the organic IL cations remain intact. However, the appearance of a resonance at δ 3.70 ppm in the ^1H NMR spectra of the recycled ILs corresponds to unreacted ethylene glycol, illustrating that the washing step does perfectly purify the IL. ^1H NMR spectra were taken before and after washing the miscible ILs in the continuous flow recycler (Fig. S2, ESI†), which show that *ca.* 50–80% of the starting ethylene glycol is removed after purification for all three OTf^- ILs. This demonstrates that while the continuous flow purification is not quantitative, it does have some success in removing polar reaction impurities. The XRD patterns and TEM images of the Pt nanoparticles synthesized in the virgin and recycled ILs with the OTf^- anion are given in Fig. S3 in the ESI.† The XRD patterns confirm the synthesis of phase pure, face-centered cubic Pt nanoparticles from each of the experiments with virgin ILs. However, a significant decrease in nanoparticle crystallinity is observed as recycled IL is used through multiple

syntheses. TEM images of Pt nanoparticles synthesized in each virgin, 1× recycled, and 5× recycled IL solvent with the OTf^- anion are shown in Fig. S3 in the ESI.† Again, as a result of the less efficient purification, the Pt nanoparticle sizes and polydispersity increase upon multiple reuses of the ILs with the OTf^- anion.

BMIM-OTf results in an isolated Pt nanoparticle yield of 14%, BMPYRR-OTf results in an isolated yield of 94%, and BMPY-OTf results in an isolated yield of 10%. Interestingly, the IL solvents with the $BMPYRR^+$ cation give the highest isolated yields of Pt nanoparticles for both NTf_2^- and OTf^- anions. However, unlike the ILs with the NTf_2^- anion, the isolated yields for the IL solvents with the OTf^- anion do not remain constant through recycling. After five recycles, the isolated yield achieved with BMIM-OTf increases to 70%, the isolated yield achieved with BMPYRR-OTf increases to 160%, and the isolated yield achieved with BMPY-OTf increases to 68%. This increase in yield can be attributed to ineffective stripping of Pt from the used IL, resulting in carryover of Pt-containing species in the ILs. Such increases in apparent Pt nanoparticle yields caused by Pt carryover resulting from ineffective extraction and purification have been reported previously.[17] These results further illustrate the importance of efficient liquid–liquid extraction for the recyclability and employment of these IL solvents.

Techno-economic analysis

We performed an early-stage economic assessment of the synthesis of Pt nanoparticles using the six IL solvents described above with CatCost, a free cost estimation tool,[45,46] to assess the impact of IL recycling on the overall synthesis costs. Estimates were made for the cost of a model catalyst material consisting of Pt nanoparticles supported on porous carbon at 0.5 wt% (0.5 wt% NP-Pt/C), as an approximation for a commercial application of the Pt nanoparticles. All the cost estimates for this analysis are reported in USD with 2016 as the pricing basis year. Table 2 summarizes the results for all the ILs used in this study. The IL recovery yield was determined experimentally as the average recovery yield of all five recycles for a given IL.

The starting point for this analysis was calculating the total cost of each NP-Pt/C system using virgin ILs. The NP-Pt/C costs using these six virgin ILs differ dramatically (*i.e.*, from $11 957 per kg NP-Pt/C for BMPY-OTf to $559 per kg NP-Pt/C for $BMPYRR\text{-}NTf_2$) because of the large range of IL bulk prices (*i.e.*, from $441 per kg NP-Pt/C for BMPY-OTf to $187 per kg NP-Pt/C for $BMPYRR\text{-}NTf_2$) and significant differences in the isolated Pt nanoparticle yield (*i.e.*, from 10% for BMPY-OTf to 98% for $BMPYRR\text{-}NTf_2$). Given this large range of nanoparticle yields, it is perhaps unsurprising that the virgin IL with the highest yield ($BMPYRR\text{-}NTf_2$) has the lowest catalyst cost ($4673/kg), while the virgin IL with the lowest yield (BMPY-OTf) has the highest ($53 199/kg). This highlights the significant differences that arise and must be considered when adapting a synthetic process to a different solvent system. Without recycling, in all cases the cost of the virgin IL solvent contribute more to the catalyst cost than even K_2PtCl_4, with the most extreme cases being closer to 10× greater (*e.g.*, BMPY-OTf). While perhaps counterintuitive, this result underscores the challenge in the commercialization of processes that utilize ILs in a once-through synthesis and highlights the importance of early-stage economic assessment to identify the greatest cost drivers instead of assuming it is the platinum-group metal being used.

This techno-economic analysis gives insight into the cost savings that can be achieved with recycling. With implementation of solvent recycling using our continuous flow recycler, the solvent costs of the ILs per kg NP-Pt/C are all substantially reduced relative to the virgin IL analogues. For example, using virgin $BMPY\text{-}NTf_2$ results in the third highest reaction solvent cost ($5271 per kg NP-Pt/C) as well as the third highest total cost reported ($22 502 per kg NP-Pt/C). These costs are in part driven by a modest Pt nanoparticle yield (24%). Recycling this IL with a solvent recovery yield of 94% results in a reaction solvent cost that is 20× cheaper ($269) and a total cost that is close to half of that using the virgin IL. Using recycled IL results in >90% savings of the reaction solvent cost for almost all ILs, with the exception of BMPYRR-OTf having an 81% solvent cost reduction per kg NP-

Table 2 Estimated costs for 0.5 wt% Pt/C nanoparticles prepared with various reaction solvents including virgin ILs and 5× recycled ILs[a]

Inputs			Costs (2016 $ per kg NP-Pt/C)					
Reaction solvent	Reaction yield	IL recovery	Reaction solvent	K_2PtCl_4	Other materials	Processing	Margin	Total
Virgin $BMIM\text{-}NTf_2$	36		1912	356	192	10 600	101	13 161
Recycled $BMIM\text{-}NTf_2$	38	91%	118	337	179	10 583	104	11 321
Virgin $BMPYRR\text{-}NTf_2$	98		559	131	83	3863	37	4673
Recycled $BMPYRR\text{-}NTf_2$	98	94%	38	131	68	4094	40	4371
Virgin $BMPY\text{-}NTf_2$	24		5271	533	278	16 268	152	22 502
Recycled $BMPY\text{-}NTf_2$	31	90%	269	413	216	12 995	127	14 020
Virgin BMIM-OTf	14		5630	915	462	27 386	260	34 653
Recycled BMIM-OTf	70	65%	366	183	96	5784	56	6485
Virgin BMPYRR-OTf	94		1070	136	85	4102	38	5431
Recycled BMPYRR-OTf	160	70%	204	80	42	2529	25	2880
Virgin BMPY-OTf	10		11 957	1280	640	38 958	364	53 199
Recycled BMPY-OTf	68	63%	571	188	98	5984	57	6898

[a] The processing column includes all non-materials costs, such as utilities, operating expenditures, and capital expenditures. Most of the processing costs for these syntheses is contributed by labor and related operating costs.

Pt/C. However, because of the differences in water miscibility, the driving factor of the solvent cost reduction differs between ILs with NTf_2^- and OTf^- anions. Because the ILs with the NTf_2^- anion are water-immiscible, the separation and purification process in the continuous flow recycler is quite successful in removing reaction byproducts. This is validated by the absence of impurities in the solution NMR spectra, the fact that the isolated Pt nanoparticle yield does not increase upon using recycled IL, and the relatively high solvent recovery yield of ≥90%. From this, we can conclude that the solvent cost reduction is predominantly driven by recycling. In contrast, the IL solvents with the OTf^- anion are miscible with water, making the purification and separation in the continuous flow recycler less efficient. This is demonstrated by the presence of ethylene glycol in the solution NMR spectra of the recycled ILs, an increase of the Pt nanoparticle yield upon using recycled IL, and a relatively low solvent recovery yield of 63–70%. From this, we conclude that the solvent cost reduction for the ILs with the OTf^- anion is mainly driven by an increase in Pt nanoparticle yield upon successive recycles, as this means less IL is needed to produce the same amount of catalyst.

Another significant detail realized from the techno-economic analysis is that the solvent costs per kg NP-Pt/C using recycled IL solvents with the NTf_2^- anion (*i.e.*, recycled BMIM-NTf_2, BMPYRR-NTf_2, and BMPY-NTf_2) become cheaper than the K_2PtCl_4 precursor price per kg NP-Pt/C. However, the experimental–economic approach performed using the virgin ILs demonstrates that the reaction solvent cost is higher than the cost of the K_2PtCl_4 precursor per kg NP-Pt/C. This illustrates how costly and untenable it can be to employ once-through virgin IL solvents. To further highlight the impact of solvent recycling, Fig. 4 shows the relative cost contributions from the reaction solvent, the K_2PtCl_4 precursor per kg NP-Pt/C, and other materials used in the Pt nanoparticle synthesis (*e.g.*, PVP, ethylene glycol, work-up solvents, *etc.*) for both virgin and recycled ILs. Upon recycling, the K_2PtCl_4 precursor per kg NP-Pt/C becomes the largest cost contributor out of the three components. This is driven by a significant reduction in IL solvent cost. That is, for BMIM-NTf_2, the reaction solvent cost is reduced from 78% to 19%, for BMPYRR-NTf_2, the reaction solvent cost is reduced from 72% to 16%, and for BMPY-NTf_2 the reaction solvent cost is reduced from 87% to 30% per kg NP-Pt/C.

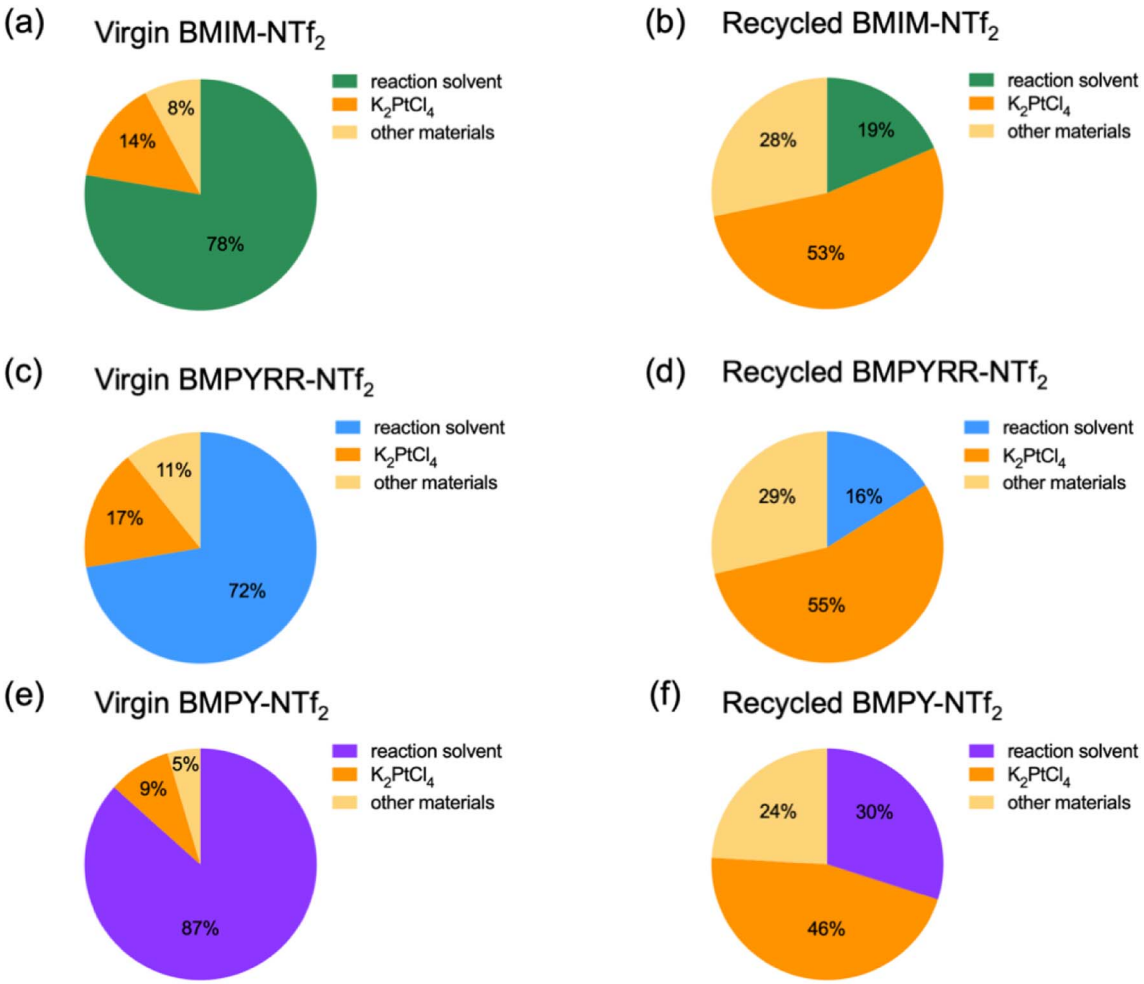

Fig. 4 Contribution of major cost drivers resulting from Pt nanoparticle syntheses using virgin and recycled (a and b) BMIM-NTf_2, (c and d) BMPYRR-NTf_2, and (e and f) BMPY-NTf_2, respectively.

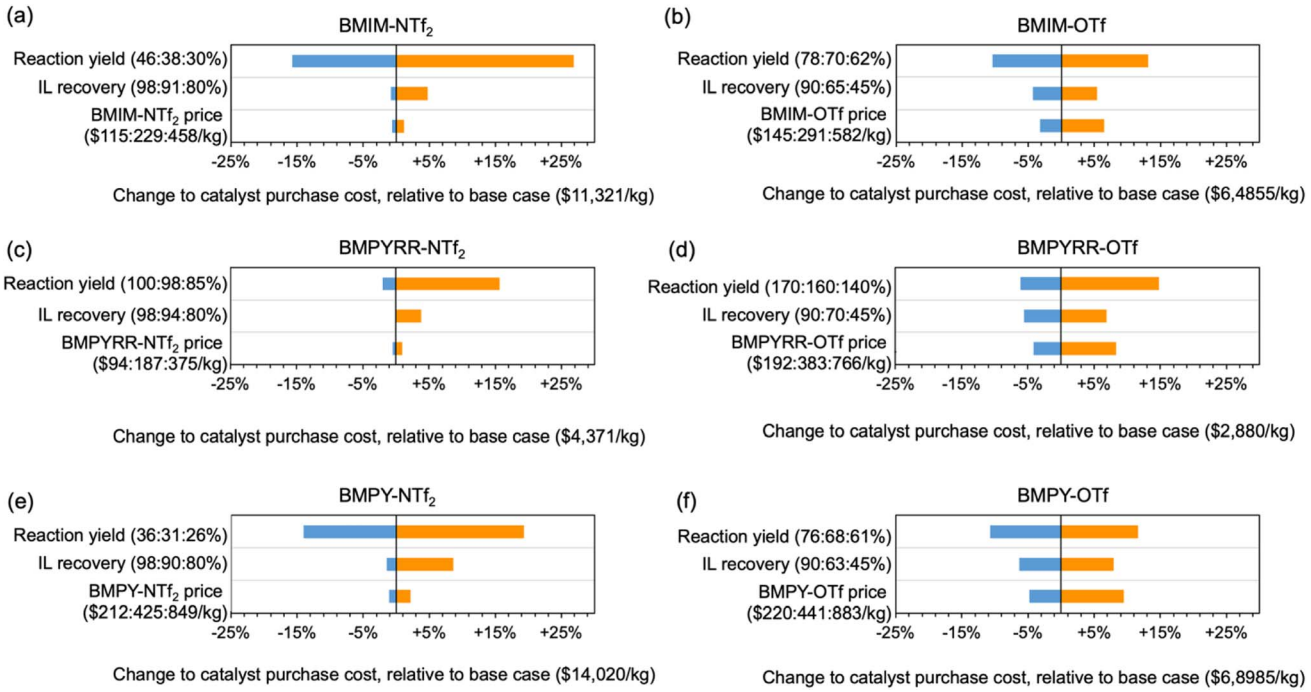

Fig. 5 Tornado plot showing the results of the sensitivity analysis on the cost of 0.5% NP-Pt/C using (a) BMIM-NTf_2, (b) BMIM-OTf, (c) BMPYRR-NTf_2, (d) BMPYRR-OTf, (e) BMPY-NTf_2, and (f) BMPY-OTf.

The sensitivity of the catalyst synthesis cost to the cost factors specific to each IL is illustrated by a sensitivity analysis evaluating how isolated Pt nanoparticle yield, IL recovery yield, and bulk price of the IL can affect the final NP-Pt/C cost. Fig. 5 shows this sensitivity analysis for all six of the IL solvents, using the recycled IL as the baseline scenario in each case. The analysis illustrates the percent change to the NP-Pt/C cost relative to the baseline case. Across all six IL solvents, the isolated yield of Pt nanoparticles has the largest effect on NP-Pt/C cost, ranging from *ca.* −15% to +25%. A higher Pt nanoparticle yield means less Pt precursor is required to make the same amount of catalyst and the overall cost of the NP-Pt/C catalyst will decrease. The effect of nanoparticle yield on catalyst cost has also been reported previously.[17,47] Furthermore, the relative importance of the other two factors (*i.e.*, IL recovery yield and bulk IL price) is heavily dependent on the particular anion. The ILs with the NTf_2^- anion follow a similar trend in that the IL recovery yield has a greater effect than the bulk IL price, whereas for the ILs with the OTf^- anion, the bulk IL price has a greater effect than the IL recovery yield. The IL solvents with the OTf^- anion are recovered at significantly lower rates than the ILs with the NTf_2^- anion, meaning that the bulk price of the IL has a larger effect on the overall purchase costs because more virgin IL is needed to replenish the solvent volume in each subsequent reaction. Again, this difference highlights the fact that IL miscibility plays a very important role in the overall NP-Pt/C costs.

Conclusions

This study demonstrates a method for identifying a process-cost idealized IL solvent for a colloidal nanoparticle synthesis based on solvent cost, reaction yield, and capacity for solvent recycling. We established a matrix of six ILs as solvents for the model colloidal synthesis of Pt nanoparticles. These ILs were recovered and purified in a continuous flow recycler with acidified water and reused in subsequent nanoparticle syntheses without any chemical degradation to the IL structure. An early-stage techno-economic analysis illustrates that IL recycling can eliminate the economic barrier to unlocking the sustainability advantages of using IL solvents over traditional VOC solvents. A sensitivity analysis was performed to examine the influence of different input parameters (*i.e.*, isolated yield of Pt nanoparticles, IL recovery yield, and bulk IL price) on an overall NP-Pt/C catalyst cost. This analysis revealed that the main cost contributor across all six ILs is the nanoparticle isolated yield, which can change the cost on the order of *ca.* −15 to +25% relative to the baseline scenario. The order of the other two cost contributors is directly dependent on the IL anion, which further highlights the fact that the miscibility of ILs is imperative to efficient separation and purification.

Performing this early-stage techno-economic analysis on the factors that affect the cost of employing and recycling ILs gives important information about specific choices that should be made when scaling up. For example, the bulk price of ILs is not the only factor that should be considered. ILs have different abilities to be recycled and reused in subsequent reactions. Their miscibility with polar solvents plays a large role in the success of purification when attempting to use water as a washing agent. IL solvents also affect the reaction chemistry to differing degrees, stemming from their dual properties of acting as a solvent and interacting with the nanoparticles as surface stabilizers, which in turn affects the isolated yields and quality

of the nanoparticles. For example, using recycled BMPYRR-OTf results in the lowest overall cost of NP-Pt/C ($2880), but the quality of the resulting Pt nanoparticles is significantly compromised relative to using virgin BMPYRR-OTf. By combining techno-economic and materials characterization data, the best task specific IL can be chosen. In this case, recycled BMPYRR-NTf_2 would be chosen because of its relatively low cost and superior quality of the resulting Pt nanoparticles. This highlights the importance of using cost information in a combined experimental–economic approach to assist in minimizing the overall synthesis cost and provide the context in which task specific ILs can be identified and adapted at scale, bridging the gap to implement ILs industrially and benefit from their sustainability advantages.

Experimental procedures

Platinum nanoparticle synthesis

K_2PtCl_4 (99.9%; Sigma-Aldrich), polyvinylpyrrolidone (PVP) (MW = 55 000; Aldrich), and ethylene glycol (99.8%; Sigma-Aldrich) were all used as received. 1-Butyl-3-methylimidizolium bis(trifluoromethylsulfonyl)imide (BMIM-NTf_2, 99%, Lot # W006x106.2.1), 1-butyl-3-methylimidazolium triflate (BMIM-OTf, 99%, Lot # T009x88.7), 1-butyl-1-methylpyrrolidinium bis(trifluoromethylsulfonyl)imide (BMPYRR-NTf_2, 99%, Lot # T009x88.1), 1-butyl-1-methylpyrrolidinium triflate (BMPYRR-OTf, 99%, Lot # P00364.1), 1-butyl-2-methylpyridinium bis(trifluoromethylsulfonyl)imide (BMPY-NTf_2, 99%, Lot # F00113.1), and 1-butyl-2-methylpyridinium triflate (BMPY-OTf, 99%, Lot # Q00188.1) were all purchased from IoLiTec and dried under vacuum at 120 °C for 2 h prior to use. In a standard procedure, 42.1 mg (0.100 mmol) of K_2PtCl_4 was dissolved in 2.7 mL of ethylene glycol. Separately, 227.2 mg of PVP was added to 8.0 mL of the IL in a two-neck round bottom flask equipped with a condenser and septum. The PVP was dissolved in the IL by heating it in a thermostatically controlled oil bath at 150 °C for 10 min, giving a clear solution. The solution of K_2PtCl_4 in ethylene glycol was then hot injected into the IL solution of PVP and the reaction solution was maintained at 150 °C for 30 min. The solution was thermally quenched in an ice bath. For the three IL solvents with NTf_2^- anions, the reaction mixture was transferred to a 30 mL separatory funnel. After complete phase separation, the IL layer (bottom) was separated from the black Pt nanoparticle suspension in ethylene glycol (top) and subsequently washed with acidified water in the continuous flow recycler (*vide infra*). The black Pt nanoparticle suspension (2.7 mL) was equally split between two 50 mL centrifuge tubes and precipitated with 30 mL of acetone in each tube followed by centrifugation (6000 rpm or 3820 × *g*, 5 min). The clear supernatant was decanted, and the solid product was redispersed in 10 mL of ethanol and precipitated with 30 mL of hexanes followed by centrifugation (6000 rpm or 3820 × *g*, 5 min). Dispersion in ethanol and precipitation with hexanes was performed two more times. The final Pt nanoparticle product was redispersed in ethanol to give a stable colloidal suspension or dried under nitrogen for further characterization. For the three IL solvents with the OTf^- anions, the reaction mixture was transferred to a 50 mL centrifuge tube and 30 mL of acetone was added to precipitate the Pt nanoparticles. The supernatant containing the IL was saved, and the acetone and other volatiles were removed *in vacuo*. The IL was then washed with acidified water in the continuous flow recycler with an IL membrane separator. The Pt nanoparticles were then purified three times with 10 mL of ethanol and 30 mL of hexanes *via* centrifugation (6000 rpm or 3820 × *g*, 5 min). The isolated Pt nanoparticle yield was calculated from the residual Pt mass determined by thermogravimetric analysis (TGA). The experimental error of calculating isolated yield from TGA is ± 2 wt%.

Fabrication of continuous flow microfluidic recycler

The continuous flow recycler was designed in Autodesk Inventor Profession 2022 and fabricated *via* stereolithography (SLA) by a 3D printer (model MAX X UV 385; Asiga) with a transparent methacrylate-based resin (GR-10; Pro3dure Medical). The as-printed device was washed in three sequential isopropanol (Supelco) baths to flush away excess uncured resin right after being removed from the print bed. Isopropanol was also injected inside the device by hand to flush the microchannel. The device was air dried for 5 min before using. A hydrophobic PTFE membrane (pore-size 100 nm; Sterlitech) was placed in between the two parts of the recycler that were then combined by a quick-cure epoxy (Bob Smith Industries). After 2 h of epoxy curing, 200 μL of NTf_2^- ILs were infused into the recycler to pre-wet the membranes. The cation of the pre-wetting ILs corresponded to the cation of the IL-to-purify (*e.g.*, BMIM-NTf_2 to pre-wet recyclers for purifying BMIM-NTf_2 and BMIM-OTf). Drawings and measurements of the recycler are provided in the ESI.†

Washing of water-immiscible ionic liquids in continuous-flow recycler

Nitric acid (70%) was diluted in deionized water to give a 0.1 M acidified aqueous solution. The water-immiscible NTf_2^- IL feed stream and acidified water feed stream were loaded in two separate 20 mL syringes (Luer-lok; BD). Two syringe pumps (Fusion 200; Chemyx) in infusion mode were used to inject the two streams into the recycler (IL flow rate = 100 μL min; acidified water flow rate = 130 μL min^{-1}). The stream formed biphasic slug flow and passed through 41 cm-long channel (herringbone and wavy) where extraction occurred. The slug flow then passed through a separation section where membrane separation occurred. The permeate IL phase was collected from the lower outlet of the recycler, while the retentate aqueous phase was collected to a 20 mL syringe loaded on a third syringe pump in withdrawal mode (flow rate = 129 μL min^{-1}). PTFE tubing (I.D. 1/32 in; Cole-Parmer) was used to connect all syringes and the recycler (length from IL syringe to recycler port = 10 cm; from acidified water syringe to recycler port = 10 cm; from recycler upper outlet to waste aqueous syringe = 15 cm; from recycler lower port to IL product outlet = 5 cm). Nuts and ferrules selected in appropriate sizes for all connections were purchased from IDEX Health & Science. The IL phase going into the withdrawal syringe due to retention before steady state was also collected to minimize loss. The one-time washed IL

product was then reloaded into a new 20 mL syringe for the second wash to proceed following the same procedure described above. A third wash was carried out after the same workup procedure after the second wash. The three-time purified, recycled IL product was dried under vacuum at 120 °C for 2 h to remove any bulk residual water. An appropriate amount of fresh IL was added to each synthesis to ensure the reaction volume remained consistent.

Washing of water-miscible ionic liquids in continuous-flow recycler

The experimental setups for the three water-miscible IL solvents with OTf^- anions followed the same procedure as that for the NTf_2^- ILs. The OTf^- IL stream and 0.1 M acidified aqueous stream were infused into the recycler with flow rates of 100 μL min^{-1} and 11 μL min^{-1}, respectively. The retentate aqueous waste was collected by the syringe pump in withdrawal mode at flow rate of 11 μL min^{-1}. The IL product from the lower outlet of the recycler was then reloaded to the infusion pump to conduct the second and third washes. The three-time washed and recycled IL product was dried under vacuum at 120 °C for 2 h to get rid of any residual water and other volatiles. An appropriate amount of fresh IL was added to ensure the reaction volume remains consistent.

Supported nanoparticle cost estimation

Cost estimates were compiled in Microsoft Excel v16 using the spreadsheet version of CatCost v1.0.4.[45] A full description of all assumptions, including input costs, cost factors, and other variables, is provided in the ESI.† All prices were adjusted to 2016 USD by use of the U.S. Bureau of Labor Statistics Chemical Producer Price Index (ChemPPI) or, for equipment costs, the Chemical Engineering Plant Cost Index. Raw materials prices at 1000 kg order size or greater were estimated through a combination of vendor quotations, freely available and proprietary price databases, and estimates from industry experts. Generally, several sources were consulted to develop an average and/or verify each assumed price. A factor of 3% was added to the raw materials costs to account for waste and spoilage. Processing costs were estimated using the CapEx & OpEx factors method. For the CapEx & OpEx factors method, the equipment list is detailed in the ESI.† The remainder of the capital costs—including direct capital costs like installation, piping, instrumentation, and buildings; indirect costs like engineering, legal, and contingencies; and working capital—were estimated as fixed factors (multipliers) of the total purchased equipment cost using the modified Lang factors[48,49] of Peters and Timmerhaus.[50] A similar calculation approach and factors were taken from the same source[50] to determine operating costs such as supervisory labor and maintenance supplies, fixed/indirect costs such as insurance and overhead, and general expenses such as distribution and marketing. Direct labor was calculated by summing the labor factors of all the equipment items after scaling to the specified production rate, then rounding up to the nearest whole number to determine number of operators. Year-round operation (8760 h) with full staffing during maintenance downtime was assumed. A labor rate including benefits of $48/h for US Gulf Coast production was used. The value of the spent catalyst, which was estimated at $111.34/kg for all the catalysts, was not included in the analysis; all cost estimates reflect the purchase cost. The supporting procedures to generate 0.5 wt% NP-Pt/C (*i.e.*, addition of as-synthesized Pt nanoparticles to a carbon support by dropcasting) are included in the cost estimates. Targeting a specific metal loading from Pt nanoparticle suspensions (*e.g.*, 0.5 wt% Pt/C) can be done through a ligand weight-correction *via* thermogravimetric analysis to obtain the Pt metal content in each sample. This procedure has been previously reported for successfully targeting a specific metal loading for a given supported catalyst.[51,52]

Characterization

Powder X-ray diffraction (XRD)

XRD patterns were collected on a Rigaku Ultima IV diffractometer operating with a Cu Kα X-ray source ($\lambda = 1.5406$ Å) at 40 mA and 44 kV.

Transmission electron microscopy (TEM)

TEM images were acquired with a JEOL JEM2100F (JEOL Ltd.) microscope operating at 200 kV. Each sample was drop-cast on 400 mesh Cu grids coated with a lacey carbon film (Ted Pella, Inc.) and dried overnight under vacuum at room temperature. The average sizes of the Pt nanoparticles were determined using *ImageJ*, a pixel-counting software ($N = 300$).

Thermogravimetric analysis (TGA)

Thermogravimetric analysis of the Pt nanoparticles was performed on a TGA Q50 instrument. The organic-corrected, isolated yield of Pt nanoparticles from each reaction was gravimetrically calculated *via* TGA. To determine the organic ligand content, *ca.* 10 mg of Pt nanoparticle powder isolated after workup was heated to 700 °C under flowing air at a heating rate of 10 °C min^{-1}.

Nuclear magnetic resonance (NMR) spectroscopy

Solution ^1H and ^{19}F NMR spectra were collected on a Varian 600 MHz VNMRS spectrometer using 16 scans. $CDCl_3$ was used as the deuterated solvent. All the sample concentrations in the NMR tubes were kept constant with the addition of 5 μL of IL into 800 μL of $CDCl_3$.

Conflicts of interest

The authors declare no competing financial interest.

Acknowledgements

The experimental work by N. M. and R. L. B. was supported by the National Science Foundation (grant CMMI-1728649). This work was authored in part by the National Renewable Energy Laboratory, operated by Alliance for Sustainable Energy, LLC for the U.S. Department of Energy (DOE) under Contract No. DE-

AC36-08GO28308. This research was conducted in collaboration with the Chemical Catalysis for Bioenergy (Chem-CatBio) Consortium, a member of the Energy Materials Network (EMN). Funding was provided by the US DOE Office of Energy Efficiency and Renewable Energy Bioenergy Technologies Office. The views expressed in this article do not necessarily represent the views of the DOE or the U.S. Government. The U.S. Government retains and the publisher, by accepting the article for publication, acknowledges that the U.S. Government retains a nonexclusive, paid-up, irrevocable, worldwide license to publish or reproduce the published form of this work, or allow others to do so, for U.S. Government purposes.

References

1 M. Freemantle, *Chem. Eng. News*, 1998, **76**, 32–37.
2 G. Choudhary, J. Dhariwal, M. Saha, S. Trivedi, M. K. Banjare, R. Kanaoujiya and K. Behera, *Environ. Sci. Pollut. Res.*, 2023, DOI: 10.1007/s11356-023-25468-w.
3 N. V. Plechkova and K. R. Seddon, *Chem. Soc. Rev.*, 2008, **37**, 123–150.
4 T. Welton, *Chem. Rev.*, 1999, **99**, 2071–2084.
5 R. Giernoth, *Angew. Chem., Int. Ed.*, 2010, **49**, 2834–2839.
6 R. Jin, C. Zeng, M. Zhou and Y. Chen, *Chem. Rev.*, 2016, **116**, 10346–10413.
7 S. E. Lohse and C. J. Murphy, *J. Am. Chem. Soc.*, 2012, **134**, 15607–15620.
8 J. Dupont and P. A. Z. Suarez, *Phys. Chem. Chem. Phys.*, 2006, **8**, 2441.
9 J. Dupont and J. D. Scholten, *Chem. Soc. Rev.*, 2010, **39**, 1780.
10 J. Gao, R. S. Ndong, M. B. Shiflett and N. J. Wagner, *ACS Nano*, 2015, **9**, 3243–3253.
11 V. Kamysbayev, V. Srivastava, N. B. Ludwig, O. J. Borkiewicz, H. Zhang, J. Ilavsky, B. Lee, K. W. Chapman, S. Vaikuntanathan and D. V. Talapin, *ACS Nano*, 2019, **13**, 5760–5770.
12 E. J. Roberts, C. G. Read, N. S. Lewis and R. L. Brutchey, *ACS Appl. Energy Mater.*, 2018, **1**, 1823–1827.
13 A. H. Tullo, *Chem. Eng. News*, 2020, **98**, 5.
14 X. Han and D. W. Armstrong, *Acc. Chem. Res.*, 2007, **40**, 1079–1086.
15 C. J. Wrasman, Z. Chengshuang, A. Aitbekova, E. D. Goodman and M. Cargnello, *J. Am. Chem. Soc.*, 2022, **144**, 11646–11655.
16 E. Dhaene, J. Billet, E. Bennett, I. Van Driessche and J. De Roo, *Nano Lett.*, 2019, **19**, 7411–7417.
17 L. R. Karadaghi, N. Malmstadt, K. M. Van Allsburg and R. L. Brutchey, *ACS Sustainable Chem. Eng.*, 2021, **9**, 246–253.
18 F. C. C. Oliveira, F. B. Effenberger, M. H. Sousa, R. F. Jardim, P. K. Kiyohara, J. Dupont, J. C. Rubim and L. M. Rossi, *Phys. Chem. Chem. Phys.*, 2011, **13**, 13558.
19 D. V. Wagle, A. J. Rondinone, J. D. Woodward and G. A. Baker, *Cryst. Growth Des.*, 2017, **17**, 1558–1567.
20 B. Zhang, Y. Xue, Z. Xue, Z. Li and J. Hao, *ChemPhysChem*, 2015, **16**, 3865–3870.
21 Y. Wang, S. Maksimuk, R. Shen and H. Yang, *Green Chem.*, 2007, **9**, 1051.
22 N. Bhawawet, J. B. Essner, J. L. Atwood and G. A. Baker, *Chem. Commun.*, 2018, **54**, 7523–7526.
23 C. T. Riche, E. J. Roberts, M. Gupta, R. L. Brutchey and N. Malmstadt, *Nat. Commun.*, 2016, **7**, 10780.
24 V. Mengeaud, J. Josserand and H. H. Girault, *Anal. Chem.*, 2002, **74**, 4279–4286.
25 X. Chen and T. Li, *Chem. Eng. J.*, 2017, **313**, 1406–1414.
26 A. D. Strook, S. K. W. Dertinger, A. Ajdari, I. Mezić, H. A. Stone and G. M. Whitesides, *Science*, 2002, **295**, 647–651.
27 J. Marschewski, S. Jung, P. Ruch, N. Prasad, S. Mazzotti, B. Michel and D. Poulikakos, *Lab Chip*, 2015, **15**, 1923–1933.
28 W.-Z. Lin, W. K. Bostic and N. Malmstadt, *ChemRxiv*, 2022, preprint, DOI: 10.26434/chemrxiv-2022-kgz7g.
29 J. G. Kralj, H. R. Sahoo and K. F. Jensen, *Lab Chip*, 2007, **7**, 256–263.
30 N. Weeranoppanant, A. Adamo, G. Saparbaiuly, E. Rose, C. Fleury, B. Schenkel and K. F. Jensen, *Ind. Eng. Chem. Res.*, 2017, **56**, 4095–4103.
31 J. G. McDaniel and A. Verma, *J. Phys. Chem. B*, 2019, **123**, 5343–5356.
32 M. Klähn, C. Stüber, A. Seduraman and P. Wu, *J. Phys. Chem. B*, 2010, **114**, 2856–2868.
33 O. Lanaridi, A. R. Sahoo, A. Limbeck, S. Naghdi, D. Eder, E. Eitenberger, Z. Csendes, M. Schnürch and K. Bica-Schröder, *ACS Sustainable Chem. Eng.*, 2021, **9**, 375–386.
34 Y. Tong, C. Wang, Y. Huang and Y. Yang, *Ind. Eng. Chem. Res.*, 2015, **54**, 705–711.
35 S. Génand-Pinaz, N. Papaiconomou and J.-M. Leveque, *Green Chem.*, 2013, **15**, 2493.
36 B. Pan, L. R. Karadaghi, R. L. Brutchey and N. Malmstadt, *ACS Sustainable Chem. Eng.*, 2023, **11**, 228–237.
37 P. Erfle, J. Riewe, S. Cai, H. Bunjes and A. Dietzel, *Lab Chip*, 2022, **22**, 3025–3044.
38 C. J. Clarke, L. Bui-Le and J. Hallett, *Anal. Methods*, 2020, **12**, 2244–2252.
39 V. Mazan, M. Y. Boltoeva, E. E. Tereshatov and C. M. Folden III, *RSC Adv.*, 2016, **6**, 56260–56270.
40 A. Baimoldina, F. Yang, K. Kolla, P. Altemose, B. Wang, C. Clifford, C. Kowall and L. Li, *Ind. Eng. Chem. Res.*, 2022, **61**, 747–753.
41 M. Kamaz, R. J. Vogler, M. Jebur and A. Sengupta, *Sep. Purif. Technol.*, 2020, **236**, 116237.
42 B. Wang, J. Lin, F. Wu and Y. Peng, *Ind. Eng. Chem. Res.*, 2008, **47**, 8355–8360.
43 T. H. Rehm, C. Hofmann, D. Reinhard, H.-J. Kost, P. Löb, M. Besold, K. Welzel, J. Barten, A. Didenko, D. V. Sevenard, B. Lix, A. R. Hillson and S. D. Riegel, *React. Chem. Eng.*, 2017, **2**, 315–323.
44 V. L. Rendina and J. S. Kingsbury, *J. Org. Chem.*, 2012, **77**, 1181–1185.
45 *Home | CatCost*, https://catcost.chemcatbio.org/, accessed July 28, 2022.
46 K. M. Van Allsburg, E. C. D. Tan, J. D. Super, J. A. Schaidle and F. G. Baddour, *Nat. Catal.*, 2022, **5**, 342–353.
47 B. E. Petel, K. M. Van Allsburg and F. G. Baddour, *Adv. Sustainable Syst.*, 2023, 230030.

48 H. J. Lang, Cost Relationships in Preliminary Cost Estimation, *Chem. Process Eng.*, 1947, **54**, 117–121.
49 H. J. Lang, Simplified Approach to Preliminary Cost Estimates, *Chem. Process Eng.*, 1948, **55**, 112–113.
50 M. S. Peters and K. D. Timmerhaus, *Plant Design and Economics for Chemical Engineers*, McGraw-Hill, New York, 5th edn, 2003.
51 L. R. Karadaghi, M. S. Madani, E. M. Williamson, A. T. To, S. E. Habas, F. G. Baddour, J. A. Schaidle, D. A. Ruddy, R. L. Brutchey and N. Malmstadt, *ACS Appl. Nano Mater.*, 2022, **5**, 1966–1975.
52 L. R. Karadaghi, A. T. To, S. E. Habas, F. G. Baddour, D. A. Ruddy and R. L Brutchey, *Chem. Mater.*, 2022, **34**, 8849–8857.